

SPITZER OBSERVATIONS OF THE HH 1/2 SYSTEM. THE DISCOVERY OF THE COUNTERJET

NORIEGA-CRESPO, A.¹ AND RAGA, A. C.²

Submitted 2011 December 5; accepted 2012 March 2

ABSTRACT

We present unpublished *Spitzer* IRAC observations of the HH 1/2 young stellar outflow processed with a high angular resolution deconvolution algorithm, that produces sub-arcsecond ($\sim 0.6 - 0.8''$) images. In the resulting mid-infrared images, the optically invisible counterjet is detected for the first time. The counterjet is approximately half as bright as the jet at $4.5\mu\text{m}$ (the IRAC band that best traces young stellar outflows) and has a length of $\sim 10''$. The NW optical jet itself can be followed back in the mid-IR to the position of the exciting VLA 1 source. An analysis of the IRAC colors indicates that the jet/counterjet emission is dominated by collisionally excited H_2 pure rotational lines arising from a medium with a neutral Hydrogen gas density of $\sim 1000 - 2000 \text{ cm}^{-3}$ and a temperature ~ 1500 K. The observed jet/counterjet brightness asymmetry is consistent with an intrinsically symmetric outflow with extinction from a dense, circumstellar structure of $\sim 6''$ size (along the outflow axis), and with a mean visual extinction, $A_V \sim 11$ mag.

Subject headings: circumstellar matter — stars: formation — ISM: jets and outflows — infrared: ISM — Herbig-Haro objects — ISM: individual objects (HH1/2)

1. INTRODUCTION

HH 1 and 2 were the first detected HH objects (Herbig 1951; Haro 1952). Since then, they have played an important role in the study of outflows from young stars, particularly because most of the general characteristics of HH outflows were first seen in HH 1 and 2 (see the review of Raga et al. 2011).

The first measurement of proper motions in HH objects (Herbig & Jones 1981) showed that HH 1 and 2 formed part of a bipolar outflow. The source of this bipolar outflow (centered between HH 1 and 2) was discovered in the radio continuum by Pravdo et al. (1985). This “VLA 1” source was later shown to have a jet-like structure (of $\sim 1'' \times 0''.2$, see Rodríguez et al. 2000), aligned with the HH 1/2 axis.

A jet-like structure directed towards HH1 (the “HH1-jet”) is observed at optical wavelengths (Strom et al. 1985 point out this feature, which was also visible in older images of the region). The base of this jet-like structure approaches the position of the outflow source (VLA 1) in images taken at progressively longer IR wavelengths (Roth et al. 1989).

Reipurth et al. (2000) presented optical and IR images of the HH1-jet region obtained with the HST. Their NICMOS H_2 $2.12\mu\text{m}$ and [Fe II] $1.64\mu\text{m}$ images show that the emission of the HH1-jet extends to within $\sim 2''$ from the VLA 1 outflow source. It is well known that all these multiwavelength jets are a manifestation of the same astrophysical phenomena (see e.g. the review by Raga et al. 2010). The fact that the observed HH1-jet emission does not extend to the position of the VLA 1 source and that a counterjet (directed towards HH 2) is not detected appears to be due to the presence of a dense molecular structure approximately centered on VLA 1 (see Tor-

relles et al. 1994; Choi & Lee 1998 and Cernicharo et al. 2000).

In this paper we present new *Spitzer* observations in which the counterjet (directed from the VLA 1 source towards HH 2) is detected for the first time, and ending nearly thirty years of speculation about the nature of its absence.

2. OBSERVATIONS

The observations of HH 1/2 system come from the GTO *Spitzer* Space Telescope program by Giovanni Fazio (PID 43) on the ‘Orion Streamers’ obtained with the infrared camera IRAC (Fazio et al. 2004) in February 2004. The data, consisting of the basic calibrated frames or BCDs, have been recovered from the *Spitzer* Legacy Archive, version S8.18. The original surveyed area is large and covers approximately $0.75^\circ \times 3.3^\circ$ in the four bands (1, 2, 3, 4) = (3.6, 4.5, 5.8, 8.0) μm . The data were collected using the High-Dynamic-Range (HDR) mode with a 12sec integration time for the ‘long’ frames and 0.6sec for the ‘short’ ones. For this work we have used the ‘long’ frames only, with a total integration time of 48sec per pixel.

The BCDs were then reprocessed with the HiREs deconvolution software AWAIC (A WISE Astronomical Image Co-Adder) developed by the Wide Field Infrared Survey Explorer (WISE) for the creation of their Atlas images (see e.g. Masci & Fowler 2009).³ The AWAIC software optimizes the coaddition of individual frames by making use of the Point Response Function (PRF) as an interpolation kernel, to avoid flux losses in under-sampled arrays like those of IRAC, and also allows a resolution enhancement (HiRes) of the final image, by removing its effect from the data in the deconvolution process. A similar method has been applied on the *Spitzer* data of young stellar outflows like HH 46/47 (Noriega-Crespo et al. 2004a; Velusamy et al. 2007) and Cep E

¹ Infrared Processing and Analysis Center, California Institute of Technology, CA 91125 USA

² Instituto de Ciencias Nucleares, Universidad Nacional Autónoma de México, Ap. 70-543, 04510 D.F., México

³ <http://wise2.ipac.caltech.edu/staff/fmasci/awaicpub.html>

(Moro-Martín et al. 2001; Noriega-Crespo et al. 2004b; Velusamy et al. 2011), quite successfully. On IRAC images, the HiRes processing enhances the angular resolution from the standard $\sim 2''$ to $\sim 0.6'' - 0.8''$ (Velusamy et al. 2007).

In Figures 1 and 2 we show the images of the HH 1/2 system obtained in the four IRAC bands (3.6, 4.5, 5.8 and $8.0\mu\text{m}$) before (i.e. standard coaddition of the BCDs) and after the HiRes reprocessing (iteration 25), respectively. At the iteration 25 the HiRes AWAIC processing reaches an optimal angular resolution, simultaneously preserving most of the structure of the surrounding diffuse emission, for instance that of the arc near the South of the images. Some small artifacts, however, are present in all bands, indicating that not further iterations are needed. Figure 3 shows a closer look of the $4.5\mu\text{m}$ image, where the newly discovered counterjet is the brightest, marking as well some of the well known optical knots of the HH 1 and 2 objects, and the position of the VLA 1 source. The bright infrared source along the outflow symmetry axis, the so called Cohen-Schwartz stars (C-S), that once was thought to be the driving source (Cohen & Schwartz 1979) is also indicated, plus the VLA 2 source that drives the HH 144 outflow (Reipurth et al. 1993)

One can appreciate the performance of the HiRes processing and the ability of the mid-IR observations to discover new features by comparing the processed IRAC $4.5\mu\text{m}$ with archival data at optical and near-IR observations of the HH 1/2 system obtained by the *Hubble Space Telescope*, with ~ 5 times better angular resolution (Fig. 4). The optical image was taken by the Wide Field Planetary Camera 2 (WFPC2) in 2007 (Hartigan et al. 2011) at $[\text{S II}] 6717/31 \text{ \AA}$, while the near-IR was taken with the NICMOS3 camera in 1998 at $v=1-0 \text{ H}_2 2.12\mu\text{m}$ emission line (Reipurth et al. 2000). It is quite remarkable how similar are the vibrational (at $2.12\mu\text{m}$) and rotational H_2 emission that arises from the S(9), S(10), S(11), S(12) transitions at 4.952, 4.408, 4.180 and $3.996\mu\text{m}$, covered by IRAC $4.5\mu\text{m}$ band. About halfway between the VLA 1 source and HH 2, there are two or three condensations detectable at 2.12 and $4.5\mu\text{m}$, and given their positions could belong to counter flow as well.

3. THE HH 1 JET AND COUNTERJET

A closer look of the $[\text{S II}] 6717/31 \text{ \AA}$, 2.12, 4.5 and $8.0\mu\text{m}$ emission around the jet/counter region is shown in Fig. 5. A detailed analysis of the optical and near-IR HH 1-jet properties has been carried by Reipurth et al. (2000), where they showed how the $\text{H}_2 2.12\mu\text{m}$ and $[\text{Fe II}] 1.64\mu\text{m}$ emission arise closer to the VLA 1 source, only $2.5''$ NW of it, than that of $[\text{S II}]$. Their analysis on the extinction, using the fact that the $[\text{Fe II}] 1.54\mu\text{m}$ and $[\text{S II}] 0.67\mu\text{m}$ have similar excitation energies and ionization potential, and that their ratio is nearly constant for weak shocks, allowed them to determine a 4 mag increase in the $\sim 5''$ that the nir-IR emission gets closer to the VLA 1 source.

In the mid-IR at $4.5\mu\text{m}$ both the jet and counterjet are clearly detected, and both can be traced back to the VLA 1 source. The jet/counterjet path, unfortunately, is very close to two bright infrared sources; on the NE, the C-S source and at $\sim 10''$ SE of VLA 1 by a fainter one. And so it is possible that very close to the circular

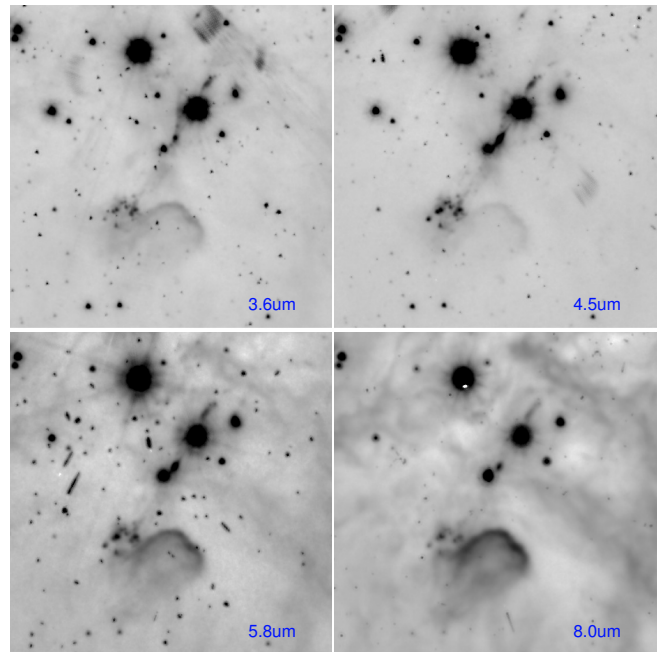


Figure 1. IRAC maps of the HH 1/2 system, from top left clockwise, at 3.6, 4.5, 5.8 and $8.0\mu\text{m}$; using a inverse grayscale where dark regions represent high intensity. The field-of-view is $\sim 5'$. North is up and East is left.

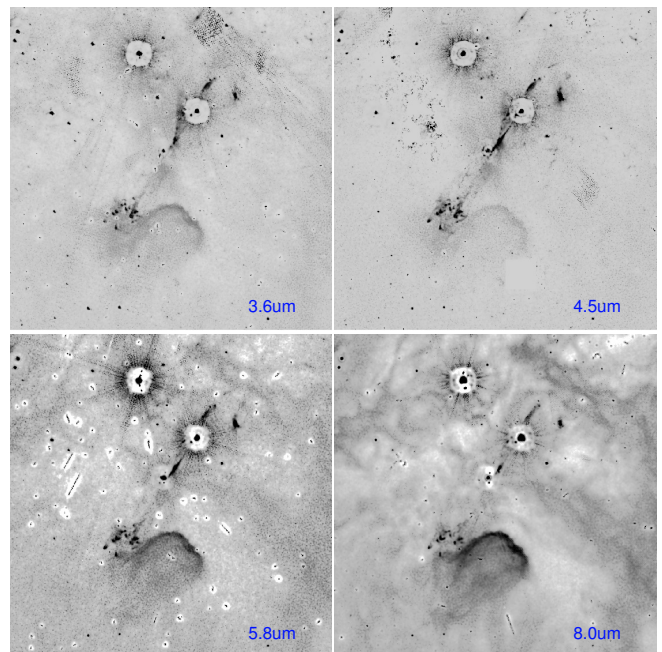


Figure 2. IRAC observations of the HH 1/2 system as in Fig 1, after 25 iterations using the HiRes AWAIC algorithm.

edges were the AWAIC HiRes algorithm suppresses the sources, that couple of knots are affected by this artifact. Conservatively, the jet has a $\sim 12.9''$ length in the NW direction arising from VLA 1, while the counterjet has a $\sim 10''$ length in the opposite direction. Both the optical and the mid-IR jet extend out to the same NW position, the A_j knot (Eisloffel, Mundt & Böhm 1994). And finally, at both 4.5 and $8.0\mu\text{m}$ couple of arcseconds NW of VLA 1, the emission broadens following the structure

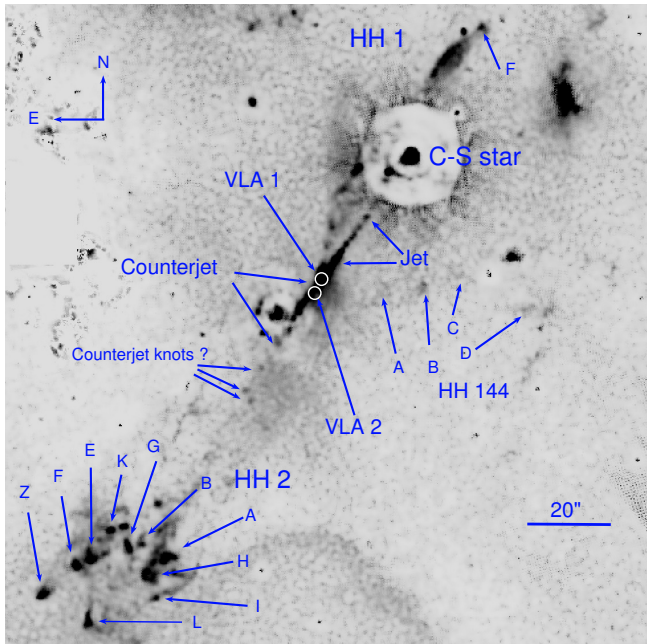


Figure 3. A closer view of the H 1/2 system at $4.5\mu\text{m}$, after the HiRes AWAIC processing, where the jet and counterjet are best detected. The names of some of the well known optical knots of HH 2 (SE) and HH 1 (NW) are included (see e.g. Raga, Barnes & Mateo 1990), as well as those of HH 144 flow (Reipurth et al. 2000) its driving source (VLA 2), and the bright IR Cohen-Schwartz (C-S) source (Cohen & Schwartz 1979).

observed at the base of the $2.12\mu\text{m}$ jet, the so called 'X' nebula (Reipurth et al. 2000). This nebula seems to be connected with the knots East of the jet; they do have a similar structure at 2.12 and $4.5\mu\text{m}$.

3.1. The Medium Surrounding the Counterjet

In Figure 6, we present 4.5 and $5.8\mu\text{m}$ intensity tracings along the jet/counterjet system. In order to obtain these tracings, we have defined an axis parallel to the direction of the outflow (the x -axis of Figure 6, with $x = 0$ corresponding to the position of the VLA 1 source, and positive x towards the NW), and averaged the intensity in a direction perpendicular to the outflow, in a box extending $\pm 3''$ to each side of the outflow axis. A background was computed from contiguous boxes on each side of the outflow (of $1''.5$ widths), and subtracted at all positions x from the axial box in order to obtain the jet emission.

The intensity tracings show that the emission from the NW jet is generally stronger than the counterjet emission. The bottom frame of Figure 6 shows the jet/counterjet intensity ratios as a function of distance from the VLA 1 source at 4.5 (left; broken line) and 5.8 (right; solid line). It is clear that the jet/counterjet intensity ratio is > 1 at $5.8\mu\text{m}$ (at all positions). At $4.5\mu\text{m}$, the jet/counterjet intensity ratio is > 1 out to $\sim 8''$ from the source, and < 1 at $\sim 10''$ from VLA 1. This region (with jet/counterjet intensity ratio < 1) is associated with the last knot along the counterjet, seen close to the stellar source $\sim 12''$ to the SE of VLA 1 (see Figures 3 and 5), and might therefore be contaminated by the deconvolved point spread function of the star. Therefore, we conclude that the observations are consistent with jet/counterjet intensity ratios > 1 at all positions both

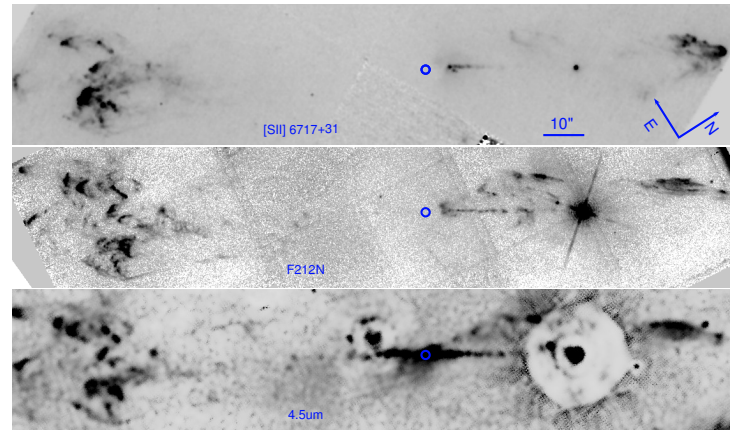


Figure 4. A comparison of the HH 1/2 system, from left to right at optical (WFPC2 [SII] $6717+31 \text{ \AA}$), near-IR (NICMOS $2.12\mu\text{m}$) and mid-IR wavelengths (IRAC $4.5\mu\text{m}$ HiRes [25 iterations] processing). The position of VLA 1 source is marked with a $3''$ in diameter circle.

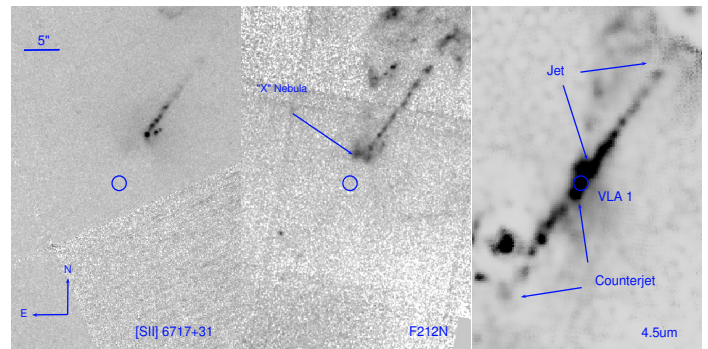


Figure 5. A closer view of the jet/counterjet region, using once again the *Hubble Space Telescope* observations in [SII] and $2.12\mu\text{m}$, and compared with those at IRAC 4.5 HiRes (25 iterations) processing. The position of VLA 1 source is marked with a $1''$ in diameter circle.

at 4.5 and $5.8\mu\text{m}$ (at least out to $\sim 8''$ from the VLA 1 source, see Figure 6). If one assumes that the jet and counterjet emission is intrinsically symmetric, one would attribute the position-dependence of the jet/counterjet intensity ratio (I_j/I_{cj} , see the bottom frame of Figure 6) to the extinction produced by a high density clump surrounding VLA 1. The fact that I_j/I_{cj} reaches a peak (with a value of ≈ 4.5 at $4.5\mu\text{m}$, and of ≈ 3 at $5.8\mu\text{m}$, see Figure 6) at $x \sim 3''$ would then indicate that the high density clump has a projected diameter of $\sim 6''$, and that for larger values of x the counterjet emerges from behind the clump (lowering the observed I_j/I_{cj} ratio). This $\sim 6''$ size is consistent with the extension along the outflow axis of the flattened H^{13}CO^+ clump observed by Choi & Lee (1998), surrounding VLA 1.

The formation of stellar outflows arising from young stellar objects (YSOs) are expected to be symmetric, since there is a preferential rotational axis and to the best of our understanding of the formation of proto-stellar jets requires a magnetohydrodynamical coupling of the accreted gas with the spherical symmetric protostar, likely to have also a symmetric bipolar magnetic structure (see e.g. Pudritz et al. 2007, and references therein). The accreted gas is provided by a disk-like structure created as a result of the original cloud spinning during the proto-

stellar collapse (see e.g. Klein et al. 2007, and references therein). One could imagine, however, that the accretion process does not need to be symmetric, and could feed the protostar in a time dependent alternative way (e.g. one star pole at the time). If this was the case, then the symmetry of the stellar jet could be broken, at least over a certain period of time, with no material ejected in one direction or another. And if this was the case then one could trace back the steps to understand where (e.g. given the morphology of the protostar’s magnetic field, or its coupling with the accretion disk or the transfer of gas and angular momentum, etc) this symmetry is broken. A true asymmetric young stellar jet could have profound consequences in our understanding of the low mass star formation process. For nearly thirty years we have wondered if the HH 1/2 system had a counterjet, although as mentioned in the introduction evidence for very dense gas ($n(\text{H}_2) = 10^4 \text{ cm}^{-3}$) structure around VLA 1, using Ammonia as a tracer (Torrelles et al. 1994), suggested that extinction was playing a major in hiding that component of the flow.

The NH_3 observations have an angular resolution of $\sim 4''$ ($\sim 2 \times 10^3$ AU at the distance of Orion), sampling very well a $2' \times 3'$ region covering the HH 1/2 outflow, and enough to distinguish a pancake-like structure perpendicular to the outflow axis and a East-West temperature gradient in it that indicates a further asymmetry. It is no a simple disk-like structure, but certainly a dense structure consistent with the idea of "a collapsing interstellar ($\sim 0.4\text{pc}$) toroid around VLA 1" (Torrelles et al. 1994). NH_3 has been used as tracer of high density and low temperature molecular gas around young stellar outflows for more than two decades. The $\text{NH}_3(1,1)$ transition requires H_2 densities higher than $5 \times 10^3 \text{ cm}^{-3}$ to be detected reliably (Torrelles et al. 1983). Typical values around YSOs range from $n(\text{H}_2) = 5 \times 10^3 \text{ cm}^{-3}$ to $\sim 10^5 \text{ cm}^{-3}$ and Temperatures of 15 - 30 K (Torrelles et al. 1983). The structure around the VLA 1 in HH 1/2 has $n(\text{H}_2) \sim 10^4 \text{ cm}^{-3}$ and 12 K. Similar conclusion was reached by Choi & Zhou (1997) using other high density molecular tracer (HCO^+). Slightly better angular resolution observations ($4.3'' \times 2.8''$ beam, Choi & Lee 1998) have traced even closer to the VLA 1 source the toroidal structure. Very close to the VLA 1 source, within a diameter of 4 AU, Cernicharo et al. 2000 estimated a very high visual extinction (80-100 magnitudes), but they were let’s concerned with the "toroidal structure". In Figure 7 we show a comparison of the $\text{NH}_3(1,1)$ observations by Torrelles et al. (1994) with the mid-IR emission at $4.5\mu\text{m}$. Two things are worth noticing, First, that high density molecular gas does indeed prevent us from detecting the counterjet at shorter wavelengths, and second, that the morphology of this dense structure is likely to prevent us to detect the HH 144 counterflow.

Independently of detailed structure of the "toroid", it is clear that a large column density of material is a long the line-of-sight of the counterjet, and this is higher than in line-of-sight of the visible jet. An estimate of the extinction around the counterjet is possible, although requires some necessary assumptions. For instance, based on symmetry one could assume that the emission properties at 3.6 and $4.5\mu\text{m}$ of jet and counterjet are very similar over the same area, and that any difference be-

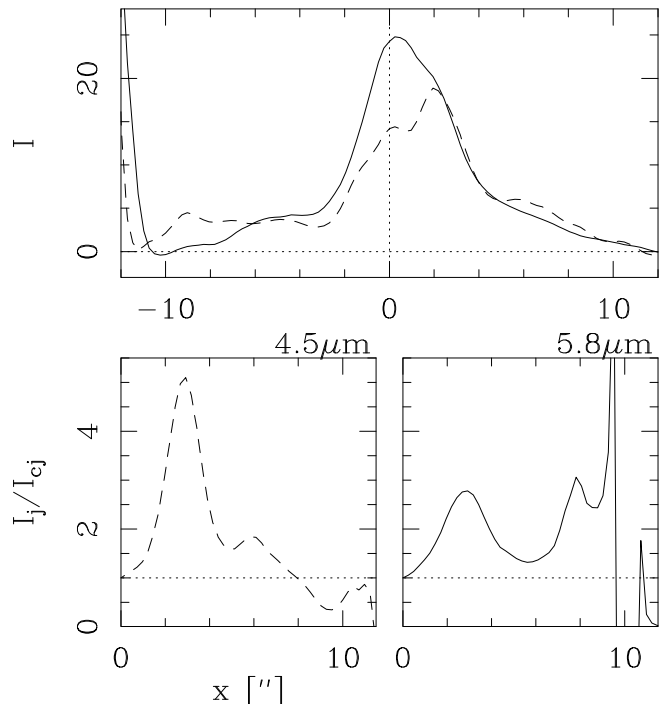


Figure 6. Top frame: surface brightness (averaged across the width of the jet, in MJy/sr) at 4.5 (dashed line) and $5.8\mu\text{m}$ (solid line) along the NW jet (positive x) and SE counterjet (negative x) centered on the VLA 1 source, showing the asymmetry of the two outflow lobes. Bottom frame: the jet/counterjet intensity ratio as a function of distance from the VLA 1 source at 4.5 (left panel; broken line) and $5.8 \mu\text{m}$ (right panel; solid line).

tween the jet (North) and the counterjet (South) are due only to extinction. A comparison of the ratio of the surface brightness of the 3.6 to $4.5\mu\text{m}$ images, indeed shows smaller values on the South with respect to the North. The average ratio of the North and South sections of the jet, using a $2.4'' \times 39.0''$ box, give values of 0.40 ± 0.27 and 0.20 ± 0.16 , respectively, i.e. the counterjet is twice as faint when compared to the jet. Two recent studies have analyzed the properties of the mid-IR extinction (Indebetouw et al. 2005, Cambresy et al. 2011), in regions located in the Galactic plane. i.e. RCW49 and the Trifid, with very similar results, so one can assume that such extinction approximately holds in the environment around the HH 1/2 system. Taking the ratios of extinction at Visual, K_s ($2.2\mu\text{m}$), 3.5 and $4.5\mu\text{m}$ to be $A_K/A_V = 0.112$, $A_{3.6}/A_K = 0.611$ and $A_{4.5}/A_K = 0.500$ (Cambresy et al. 2011), and neglecting the extinction at $4.5\mu\text{m}$ (since both jet/counterjet are detected) then at $3.6\mu\text{m}$ at the counterjet one obtains, $A_{3.6} = 0.75$, that corresponds to $A_K = 1.2$ and $A_V = 11.0$ magnitudes, respectively.

4. THE HH 1/2 MID-IR KNOTS

Since some of the first IRAC images of stellar outflows from *Spitzer* (e.g. Noriega-Crespo et al. 2004a,b, Morris et al. 2004), it has been clear that the bands at 4.5 and $5.8\mu\text{m}$ are particularly suitable to study them. There are seven pure rotational H_2 emission lines, from S(12) at $3.996\mu\text{m}$ to S(6) $6.107\mu\text{m}$ that fall within their band-passes. The $8\mu\text{m}$ band includes some bright $v=0-0$ H_2 lines (e.g. S(5) $6.907\mu\text{m}$), but the emission in this band tends to be dominated by broad band features from very

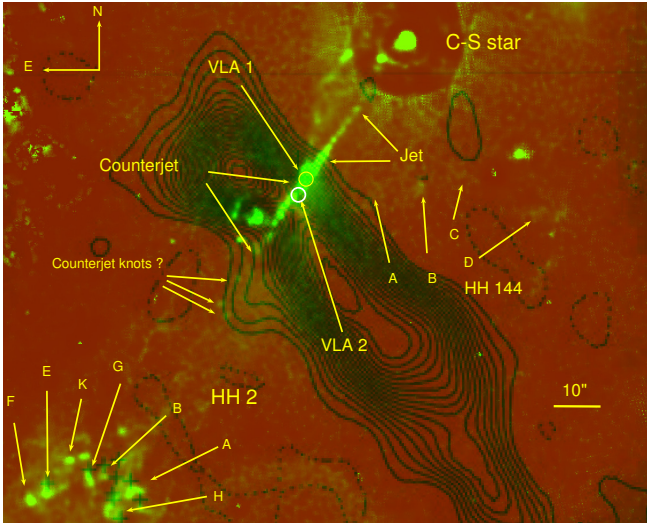


Figure 7. A comparison of the dense structure detected in $\text{NH}_3(1,1)$ at 10.5 km s^{-1} (dark contours; from Torrelles et al. 1994) with the emission at $4.5\mu\text{m}$ around the HH 1/2 jet/counterjet region.

small UV stochastically heated dust particles or Polycyclic Aromatic Hydrocarbons (PAHs) (see e.g. Tielens 2008). Recently, Ybarra & Lada (2009) have used a combination of IRAC colors to uniquely identify the thermal emission arising from collisionally excited H_2 as a function of the HI gas density and temperature, and thus provide a reliable way to study the thermal structure of the stellar outflows by using the $([3.6]-[4.5])$ and $([4.5]-[5.8])$ colors.

Some of the knots of the HH 1/2 system are clearly compact and at a first approximation one can treat them as point sources and transform their photometric fluxes into magnitudes (see e.g. “IRAC Instrument Handbook”⁴, §4.11.1, ‘Best Practices for Extended Sources’). One needs to be aware that interpreting surface brightness measurements into colors can be off by 5% - 10% (“IRAC Instrument Handbook”, §4.11.1). We adopt a 10% uncertainty across bands in our measurements, and use the standard IRAC zero points (“IRAC Instrument Handbook”, Table 4.1) of $F_{\nu 0} = 280.9, 179.7, 115.0$ and 64.9 Jy for the $3.6, 4.5, 5.8$ and $8.0\mu\text{m}$ bands, respectively. The results are presented in Table 1 and display in a color-color diagram in Figure 8, following Ybarra & Lada (2009). The diagram shows the properties of shocked excited H_2 as a function of constant HI density (dotted line) and temperature (solid line). At a temperature higher than 4000 K , the H_2 is likely to be dissociated (Ybarra & Lada 2009).

The excitation properties of the HH 1/2 knots at optical and UV wavelengths are very well known (see e.g. Solf, Böhm & Raga 1998; Solf et al. 1991; Böhm & Solf 1992; Schwartz et al. 1993; Böhm, Noriega-Crespo & Solf 1993; Moro-Martin et al. 1996; Molinari & Noriega-Crespo 2002) and are the result of their shock velocity and relative geometry. In general, high excitation knots are compact and interact through strong shocks ($60 - 100 \text{ km s}^{-1}$) with the surrounding medium, while low excitation emission arises from weaker shocks or the “wings”

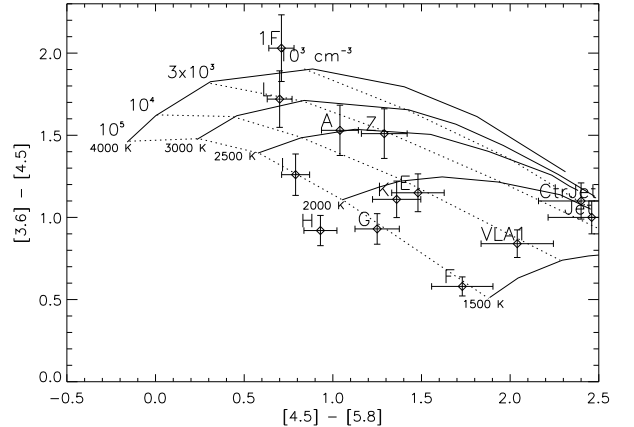


Figure 8. IRAC color-color diagram (after Ybarra & Lada 2009) of compact knots in the HH 1/2 outflow with optical counterparts, including HH 1F (1F), HH 2 (A, E, F, G, H, I, K, and Z) and regions around the jet (Jet), counterjet (CtrJet) and the VLA 1 source (see Table 1).

of bowshock-like condensations. For example, knots like HH 1F, HH 2A, HH 2G and HH 2H are high excitation, while HH 2I, HH 2L are low excitation (Raga, Böhm, & Cantó 1996). For the time variable jet, where the relative velocity between knots determines essentially the shock velocity, the overall excitation is known to be low and the shocks to be weak (Reipurth et al. 2000). Stronger shocks will produce higher post-shock gas densities and temperatures, but could also dissociate H_2 ; stronger H_2 emission indeed is expected to arise from low velocity shocks (either J-type or C-type (see e.g. Draine & McKee 1993, for a review)).

So how the properties of the mid-IR knots, dominated by emission of H_2 rotational lines at 4.5 and $5.8\mu\text{m}$, compare with those of the optical knots? One of the highest optical excitation knots, HH 1F, is slightly above the 4000 K model, the region of the diagram where indeed H_2 dissociates. The jet and counterjet, low excitation regions, do fall within the low temperature $\sim 1500 \text{ K}$ and low density ($\sim 10^3 \text{ cm}^{-3}$) models. Notice also that their IRAC colors are very close to each other, providing support to the assumption that their emission properties are nearly identical. The low excitation HH 2F and the region around VLA 1, are closer to the low 1500 K temperature model, but at higher gas density $\sim 10^5$ and 10^4 cm^{-3} , respectively. The rest of the mid-IR knots are found between these two extremes. We notice that HH 2H and G, that are along the highest density model (10^5 cm^{-3}) are also colder than the low excitation knots HH 2I and L, and this suggests that faster cooling at higher densities could play a role in reducing the excitation in the mid-IR.

5. SUMMARY AND CONCLUSIONS

We present previously unpublished *Spitzer* observations of the HH 1/2 outflow. The outflow is detected in the four IRAC channels ($3.6, 4.5, 5.8$ and $8.0\mu\text{m}$). In the $4.5\mu\text{m}$ channel, a well collimated jet/counterjet system is seen emanating from the VLA 1 radio source, which represents the discovery of the SE counterjet (previous optical and IR observations only detected the NW jet directed towards HH1).

⁴ <http://irsa.ipac.caltech.edu/data/SPITZER/docs/irac/iracinstrumenthandbook>

We find that the ratio between the jet and counterjet emission is strongly dependent on distance from the VLA 1 source. The jet/counterjet ratio is ~ 2 times larger for the $4.5\mu\text{m}$ than for the $5.8\mu\text{m}$ emission. This result is consistent an extinction effect (which would be stronger at shorter wavelengths). The fact that the jet/counterjet ratio peaks at a distance of $\sim 3''$ from the VLA 1 source indicates that the extinction is probably produced by a dense structure having an extent of $\sim 6''$ along the outflow axis. Such a dense molecular structure around VLA 1 has been observed by Choi & Lee (1998) and Cernicharo et al. (2000). We also show that the large structure of the dense gas traced by NH_3 . plays role in hidding both the HH 1/2 and HH 144 counterjets. Under the assumption that the ratio of 3.6 to $4.5\mu\text{m}$ is constant for the jet/counterjet, we estimate a $A_V = 11$ mag.

Finally, by using the IRAC colors ($[3.6] - [4.5]$) and ($[4.5] - [5.8]$) and assuming that outflow emission is dominated by shocked excited H_2 (Ybarra & Iada 2009), we show that some of the compact mid-IR knots share similar excitation properties as those of determined for the optical knots (Raga, Böhm & Cantó 1996).

We thank Frank Masci for the development of AWAIC HiRes software and making it available to us. We also thank Dr. Sean Carey for useful conversations, and the anonymous referee for her/his careful reading of the manuscript. This work is based in part on observations made with the *Spitzer Space Telescope* which is operated by the Jet Propulsion Laboratory, California Institute of Technology under NASA contract 1407. And also based on observations made with the NASA/ESA Hubble Space Telescope, and obtained from the Hubble Legacy Archive, which is a collaboration between the Space Telescope Science Institute (STScI/NASA), the Space Telescope European Coordinating Facility (ST-ECF/ESA) and the Canadian Astronomy Data Centre (CADC/NRC/CSA). The work of AR was supported by the CONACyT grants 61547, 101356 and 101975.

REFERENCES

- Böhm, K.-H. & Solf, J. 1992, *AJ*, 104, 1193
 Böhm, K.-H., Noriega-Crespo, A. & Solf, J. 1993, *ApJ*, 416, 647
 Cambresy, L., Rho, J., Marshall, D. J., & Reach, W. T 2011, *A&A*, 527, 141
 Cernicharo, J., Noriega-Crespo, A., Cesarsky, D., Lefloch, B., González-Alfonso, E., Najarro, F., Dartois, E., & Cabrit, S. 2000, *Sci*, 288, 649
 Choi, M. & Zhou, S. 1997, *ApJ*, 477, 754
 Choi, M., Lee, Y. 1998, *ApJ*, 498, L71
 Cohen, M. & Schwartz, R. D. 1979, *ApJ*, 233, 77
 Correira, J.C., Griffin, M., & Saraceno, P. 1997, *A&A*, 322, L25
 Davis, C.J., Eislöffel, J., & Ray, T. P. 1994, *ApJ*, 426, 93
 Davis, C.J., Smith, M.D. & Eislöffel, J. 2000, *MNRAS*, 318, 747
 Draine B. T. & McKee, C. F. 1993, *ARAA*, 31, 373
 García López, R., Nisini, B., Giannini, T., Eislöffel, J., Bacciotti, F., & Podio, L. 2008, *A&A*, 487, 1019
 Hartigan, P., Frank, A., Foster, J. M. et al. 2011, *ApJ*, 736, 29
 Haro, G. 1952, *ApJ*, 115, 572
 Herbig, G. H. 1951, *ApJ*, 113, 697
 Herbig, G. H., Jones, B. F. 1981, *AJ*, 86, 1232
 Indebetouw, R., Mathis, J. S., Babler, B. et al. 2005, *ApJ*, 619, 9311
 Klein, R. I., Inutsuka, S.-I., Padoan, P., & Tomisaka, K 2007, in "Protostars and Planets V", B. Reipurth, D. Jewitt, and K. Keil (eds.), University of Arizona Press, Tucson, pp.99-116
 Masci, F. & Fowler, J. W. 2009, *ASPC*, 411, 67
 Molinari, S.M. & Noriega-Crespo, A. 2002, *AJ*, 123, 2010
 Morris, P., Noriega-Crespo, A., Marleau, F. R., Teplitz, H. I., Uchida, K. I. & Armus, L. 2004, *ApJ*, 54, 339
 Moro-Martin, A., Noriega-Crespo, A., Böhm, K.-H. & Raga, A.C. 1996, *RMxAA*, 32, 75
 Moro-Martin, A., Cernicharo, J., Noriega-Crespo, A., & Martín-Pintado, J. 1999, *ApJ*, 520, L111
 Moro-Martin, A. et al. 2001, *ApJ*, 555, 146
 Noriega-Crespo, A. et al. 2004a, *ApJS*, 154, 352
 Noriega-Crespo, A. et al. 2004b, *ApJS*, 154, 402
 Noriega-Crespo, A. et al. 2011, *ApJ*, 154, 402
 Pravdo, S. H., Rodríguez, L. F., Curiel, S., Cantó, J., Torrelles, J. M., Becker, R. H., Sellgren, K. 1985, *ApJ*, 293, L35
 Pudritz, R. E., Ouyed, R., Fendt, Ch., & Brandenburg, A. 2007, in "Protostars and Planets V", B. Reipurth, D. Jewitt, and K. Keil (eds.), University of Arizona Press, Tucson, pp.277-294
 Raga, A. C., Barnes, P.J. & Mateo M. 1990, *AJ*, 99, 1912
 Raga, A.C. Böhm, K.-H. & Cantó, J. 1996, *RMxAA*, 32, 161
 Raga, A. C., Reipurth, B., Cantó, J., Sierra-Flores, M. M., Guzmán, M. V. 2011, *RMxAA*, 47, 425
 Raga, A. C., Noriega-Crespo, A., Lora, V., Stapelfeldt, K. R. & Carey, S. J. 2011, *ApJ*, 730, L17
 Reipurth, B., Heathcote, S., Roth, M., Noriega-Crespo, A., & Raga, A. C. 1993, *ApJ*, 408, 49
 Reipurth, B., Heathcote, S., Yu, K. C., Bally, J., Rodríguez, L. F. 2000, *ApJ*, 534, 317
 Rodríguez, L. F. et al. 2000, *AJ*, 119, 882
 Roth, M., Tapia, M., Rubio, M., Rodríguez, L. F. 1989, *A&A*, 222, 211
 Schwartz, R.D., Cohen, M., Jones, B.F., Böhm, K.-H., Raymond, J.C. & Hartmann, L.W. 1993, *AJ*, 106, 740
 Solf, J., Böhm K.-H. & Raga, A.C. 1988, *ApJ*, 334, 229
 Solf, J., Raga, A.C., Böhm, K.-H. & Noriega-Crespo, A. 1991, *AJ*, 102, 1147
 Strom, S. E., Strom, K. M., Grasdalen, G. L., Sellgren, K., Wolff, S., Morgan, J., Stocke, J., Mundt, R. 1985, *AJ*, 90, 2281
 Tielens, A.G.G.M. 2008, *ARAA*, 46, 289
 Torrelles et al. 1983, *ApJ*, 274, 214
 Torrelles, J. M., Gómez, J. F., Ho, P. T. P., Rodríguez, L. F., Anglada, G., Cantó, J. 1994, *ApJ*, 435, 290
 Velusamy, T. et al. 2007, *ApJ*, 668, L159
 Velusamy, T. et al. 2011, *ApJ*, 741, 60

Table 1
HH 1/2 System IRAC Colors

Knot	[3.6] - [4.5]	[4.5] - [5.8]	RA	Dec	AperRad(")
Z ^a	1.29±0.13	1.51±0.16	5h36m27.40s	-6d47m22.2s	3.0
F	1.73± 0.18	0.58± 0.06	5h36m26.84s	-6d47m15.0s	1.8
L	0.70± 0.07	1.72± 0.17	5h36m26.65s	-6d47m28.3s	3.0
E	1.48± 0.15	1.15± 0.12	5h36m26.58s	-6d47m13.2s	1.8
K	1.36± 0.14	1.11± 0.11	5h36m26.24s	-6d47m06.1s	1.8
G	1.25± 0.13	0.93± 0.10	5h36m26.00s	-6d47m10.1s	1.8
A	1.04± 0.10	1.53± 0.15	5h36m25.34s	-6d47m11.9s	2.4
H	0.93± 0.10	0.92± 0.10	5h36m25.65s	-6d47m17.2s	2.4
I	0.79± 0.08	1.26± 0.13	5h36m25.53s	-6d47m22.5s	1.8
Jet	2.46± 0.25	1.00± 0.11	5h36m22.44s	-6d45m58.1s	1.8
CtrJet	2.40± 0.24	1.10± 0.10	5h36m23.00s	-6d46m08.0s	1.8
VLA 1	2.04± 0.20	0.84± 0.09	5h36m22.83s	-6d46m05.0s	1.8
1F	0.71± 0.07	2.03± 0.20	5h36m20.23s	-6d45m05.6s	2.4

^a Knot 8 at 2.12 μ m (Davis, Eisloffel & Ray 1994)